JOURNAL OF MATERIALS SCIENCE **40** (2005) 1217– 1228

Crack growth in a new nickel-based superalloy at elevated temperature

Part I *Effects of loading waveform and frequency on crack growth*

S. DALBY
Department of Mechanical and Design Engineering, University of Portsmouth, Anglesea Road, Anglesea Building, Portsmouth PO1 3DJ, UK; Astrium Ltd., Anchorage Road, Portsmouth PO3 5PU, UK

J. TONG*
Department of Mechanical and Design Engineering, University of Portsmouth, Anglesea Road, Anglesea Building, Portsmouth PO1 3DJ, UK
E-mail: jie.tong@port.ac.uk

Crack growth at elevated temperature has been examined in a new fine-grained nickel-based superalloy under triangular, fast-slow, slow-fast, dwell and sustained loading conditions at 650 and 725°C. The effect of loading waveform seems to be minimal for base frequencies over 0.01 Hz with a mixture of time and cycle dependent crack growth observed for all but the fast-slow waveform, where the crack growth remained cycle-dependent and the crack growth rate mostly constant. For base frequencies less than 0.01 Hz, crack growth under dwell load clearly accelerated and the crack growth rates were comparable with those under sustained load. Creep contribution was found to be negligible while crack tip constraint may be relevant to the out-of-plane crack growth observed under predominantly sustained load conditions.

1. Introduction

Nickel-based superalloys have been used in aero engine turbine components since the 1940s [1]. Turbine engine discs are subjected to variable cyclic and thermal stresses during a typical loading cycle of take-off, climb, cruise and loading. Flight operations often produce loading patterns that cover a range of frequencies and waveforms, particularly in military engines where complex manoeuvres often experienced. Damage tolerance methodologies have been used for critical structural components such as turbine discs. Such approaches rely on accurate prediction of the crack growth rate under operational loading conditions. As it is impossible to reproduce all the possible loading conditions in laboratories, a systematic study of the influence of key loading variables on crack growth would seem to be necessary.

Crack growth at elevated temperature may be influenced by a number of mechanical variables, including temperature, load ratio, loading frequency and waveform. The influence of loading frequency on crack growth has been reasonably well explored [2–6]. In frequency domain, three distinct regimes have been identified as cycle-dependent, time-dependent and the mixed time/cycle dependent crack growth. Time-dependent crack growth is usually observed at low frequencies with predominantly inter-granular cracking while cycle-dependent crack growth at high frequencies with trans-granular cracking. Transitional frequencies indicate the boundaries of each regime. In comparison, however, the influence of loading waveform has not been well reported, although a significant body of work has focused on the role of dwell, or hold at the maximum load, in high temperature crack growth [7–9]. Most of the experimental data reported [10–13], however, have been obtained under constant load range control. This has severely limited the variety and the range of the selected waveforms that can be tested such that complete fracture mechanism maps for a given waveform is lacking. Furthermore, the dominant component in a given waveform with regards to crack growth is unclear. For example, the loading part of the waveform was identified as the controlling component in [10, 13]; while base frequency or total cycle time was reported to be more important in [11, 12]. This lack of a consensus may well be due to the limitation and quality of the available experimental data.

The development of nickel-based superalloys has been driven by the increasing demands for more efficient engine operation with higher operating stresses

*Author to whom all correspondence should be addressed.

and temperatures. This has led to the move from the conventional cast and wrought alloys to advanced superalloys obtained via powder metallurgy (PM) route in order to gain increased strength through higher addition of alloying elements. Compared to conventional cast and wrought alloys such as IN718 and Waspaloy, the new PM alloys have demonstrated superior tensile strength and creep resistance due to reduced grain size and more efficient γ' dispersion. However, these PM alloys also contain pores and inclusions, which make the material more susceptible to crack growth. In addition, residual stresses are often introduced during the manufacture and heat treatment processes. Consequently, poorer fatigue crack growth resistance at elevated temperature is often reported, as a result of the combination of the factors cited. Research is therefore essential to examine the crack growth resistance of the PM alloys under typical operational conditions before critical applications can be made.

This paper describes an experimental study into the effects of loading waveform and frequency on crack growth behaviour, as the first part of a trilogy. A newly developed PM nickel-based superalloy, Alloy X, was used to obtain the crack growth rate data at base frequencies spanning three decades at two temperatures, 650 and 725°C. The former represents the normal operating temperature while the latter the upper bound. Four waveforms, including balanced triangular, dwell, slow-fast and fast-slow, were examined. Crack growth under sustained loads was also studied as a limiting case of the long dwell loading conditions. Compliance methods were developed to evaluate the role of creep deformation during the crack growth. Central to the experimental programme is the constant ΔK control method, which allows a systematic study of frequency and waveform within the constraint of the time scale and the test pieces available. In Part II of this paper, numerical tools were employed to simulate the crack growth under sustained (creep) and cyclic loads. The evolution of the stress/strain fields near the crack tip under static and cyclic loads will be presented and suitable characterisation parameters will be explored. In the final Part of the paper, crack growth mechanisms were examined from a SEM analysis. A model will be presented where the mechanical variables identified in the experimental work will be explicitly incorporated and the results compared with the experimental data.

2. Experimental methods

2.1. Material and specimen

A new nickel-based superalloy, Alloy X, developed at Rolls Royce plc, has been used in this work. The chemical composition of the alloy is similar to that of U720Li alloy [5]. The alloy was solid solution strengthened using Molybdenum, Cobalt and Chromium and precipitation hardened with Aluminium and Titanium. The material was hot isostatically pressed (HIP) and extruded. A solution treatment at 1120°C for four hours was followed by a duplex aging treatment: 24 h at 650°C and air-cooling followed by 16 h at 760°C and air cool to room temperature.

TABLE I Mechanical properties of Waspaloy, U720Li and Alloy X

Temperature	Waspaloy	U720Li	Alloy X
Tensile strength (650°C)	1127 MPa	1406 MPa	1448 MPa
0.2% Yield stress (650°C)	809 MPa	1065 MPa	1034 MPa
Time to 0.1% TPS (460 MPa, 750°C)		2.79 h	45.8 h
Time to rupture (460 MPa, 750°C)		90 h	220 h

Alloy X exhibits improved tensile strength compared to those of Waspaloy and U720Li alloy, and much improved creep resistance compared to those of U720Li alloy, as shown in Table I.

Standard compact tension (CT) [14] specimens were used as received.

2.2. Microstructure

The microstructure consists of the matrix γ, a face centred cubic based on Ni with additions of alloying elements which form the strengthening secondary and tertiary precipitates γ'. Complex heat treatments were employed to control the size of the grains and precipitates. Polished and etched samples were examined at QinetiQ using filed emission gun scanning electron microscopy (FEGSEM). The grain size was measured using electron back scatter pattern (EBSP) facility and a computer-based image analysis associated with FEGSEM. The crystallographic orientation of a polished section of the material was analysed and the average grain size calculated.

The Transmission Electron Micropscopy (TEM) at Rolls Royce plc, UK, was used to examine the morphology of the secondary and tertiary γ' precipitates. Extraction replicas were prepared by mounting a section of Alloy X and polishing it to 1 μm. The sample was then etched with 10% phosphoric acid and spatter coated with Carbon. The Carbon coating was scored into 2 mm squares and etched electolytically in a solution of 20% perchloric acid in ethanol. The loosened carbon squares were then removed and placed onto copper grids. The sample was then viewed and imaged in the TEM. A linear intercept method [15] was used for the measurement of the size of the precipitates. Details of the measurement are given in [16].

2.3. Testing methods

All fatigue crack growth tests were conducted on a computer-controlled Instron servo-hydraulic testing machine (±25 KN) equipped with an electric resistance furnace. The temperature was controlled at 650 and 725 ± 2°C, with a variation along the specimen less than ±5°C. Crack lengths were monitored using a d.c. potential drop method. A pulsed d.c. current of 10A was used to ensure data acquisition at peak loads via a potential drop measurement system, Matelect. Hicks and Pickards solution [14] was employed in the crack length calibration. Prior to high temperature testing, all specimens were precracked using a decreasing ΔK scheme at room temperature. Crack growth under sustained loads was obtained using an electro-mechanical testing machine. Precracked specimens were subjected

initially to a constant cyclic load range at 0.25 Hz to gain some appreciable crack growth. The load (7 KN) was then held constant at the maximum load and crack growth was recorded as a function of elapsed time.

Constant ΔK control was used for all but sustained load tests. Values of the ΔK were chosen to lie in the mid-power law region of a fatigue crack growth rate versus ΔK plot so that the crack growth increments measured relate linearly to the number of cycles. At 650°C, the values of ΔK were chosen to be 30 and 40 MPa$\sqrt{}$m while at 725°C, $\Delta K = 25$ and 35 MPa$\sqrt{}$m were used. Varied crack morphology was created due to the different crack growth mechanisms under different loading waveforms and frequencies. The test sequences were arranged as such that distinct markings were left on the fracture surface due to the change of crack morphology. These markings were used post test to verify the measured crack length. For a given load case, the crack was allowed to grow 0.5 to 1 mm and the crack length was recorded as a function of the number of cycles from which the crack growth rate was derived from a linear regression.

Four waveforms were used in the experiments: Triangular (X-X), fast-slow (1-X), slow-fast (X-1) and dwell at maximum load (1-X-1-1). Each waveform may be described as a combination of two or more components in time, either 1 or X second(s): t_1 = ramp up, t_2 = hold at the maximum, t_3 = ramp down and t_4 = hold at the minimum. The total cycle time $t = t_1 + t_2 + t_3 + t_4$. For each waveform, at least six tests were conducted with base frequencies ranging from 0.001 to 2.5 Hz.

Compliance methods were used in the evaluation of crack closure with regard to different loading waveforms. The crack mouth opening displacement was monitored using an extensometer to assess the influence of creep deformation during crack growth.

3. Experimental results

3.1. Microstructural observation

3.1.1. Grain size

The grain sizes measured using FEGSEM are presented in Fig. 1, where each colour represents a range of grain sizes: Red, from 0–5 μm, count 465/622; green, from 5–10 μm, count 104/622; navy, from 10–15 μm, count 35/622; purple, from 15–20 μm, count 13/622; light blue, 10–25 μm, count 4/622 and pink, 25–30 μm, count 1/622. The average grain size is 3.84 μm with a standard deviation of 4.02.

3.1.2. Precipitate size

The morphology of the secondary γ' is shown in Fig. 2a while the tertiary γ' is shown in Fig. 2b. Two hundred measurements were taken from which the average size of the secondary γ' was found to be 224 ± 125 nm while the average tertiary γ' is 74 nm. While the tertiary precipitates γ' seem to be spherical the larger secondary precipitates γ' are more irregular, a change necessary to maintain its coherence within the matrix. The incoherent precipitates γ' delineate the γ-grain boundaries and these precipitates define the grain boundary characteristics and influence the fracture mode significantly.

3.2. The ΔK control method

The constant ΔK-control method requires a high level of confidence in the measured crack length. Unfortunately, errors in the instantaneous measurement during a test are not always avoidable so a post-test evaluation is essential. Each specimen was broken open after testing to allow the fracture surface to be examined and photographed. The true crack lengths were measured from the photographs. Fig. 3a shows the recorded and corrected crack length for a typical test. From the corrected values of crack length, the corrected values of ΔK were calculated and presented in Fig. 3b. Although the values of ΔK after the correction are not the same as the desired value, a constant ΔK control condition was still maintained. Fig. 3c shows the deviation of ΔK values from the desired value for a large selection of tests with a maximum relative error of less than 5%. A constant load controlled test was also carried out and the crack growth rates were found to compare well with those obtained under constant ΔK control [16].

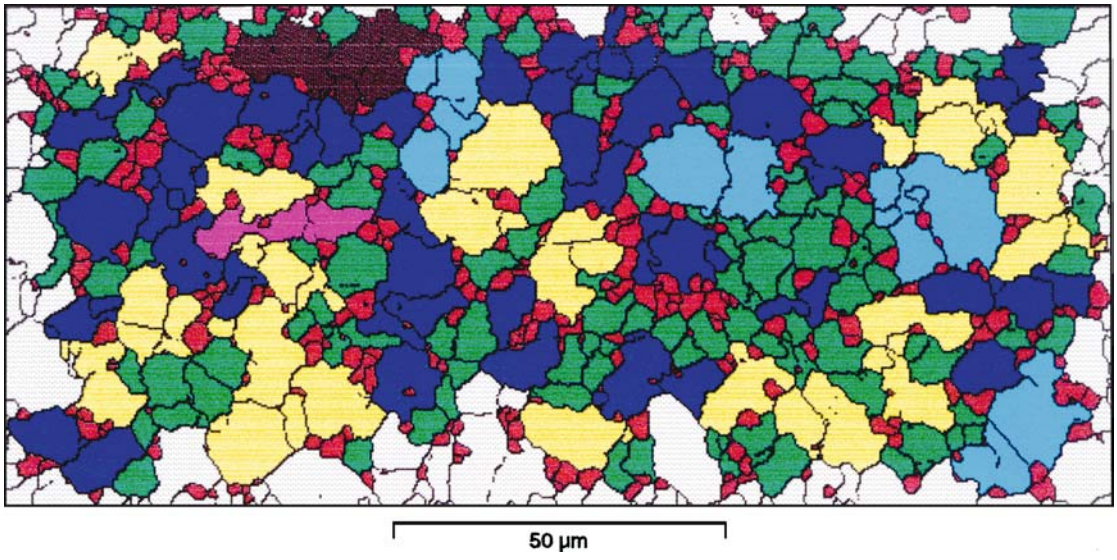

Figure 1 Grain size distribution obtained using filed emission gun scanning electron microscopy (FEGSEM).

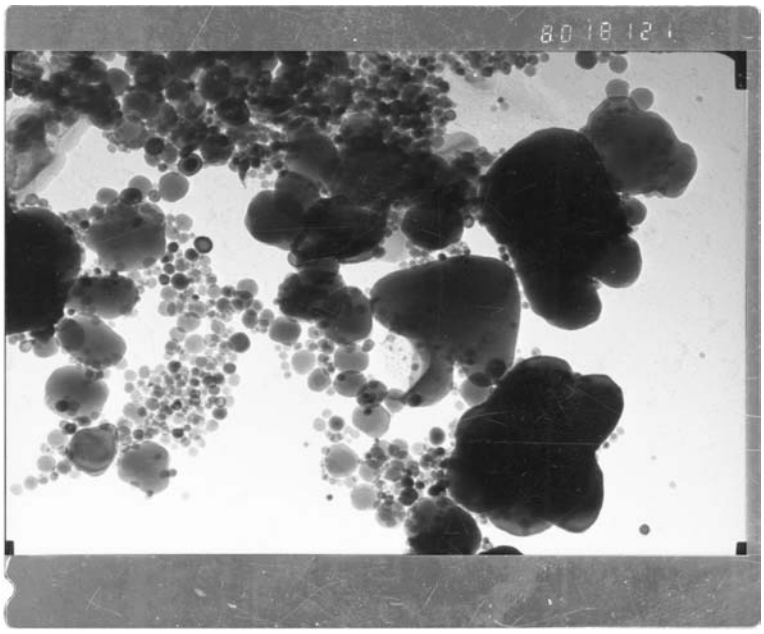

(a)

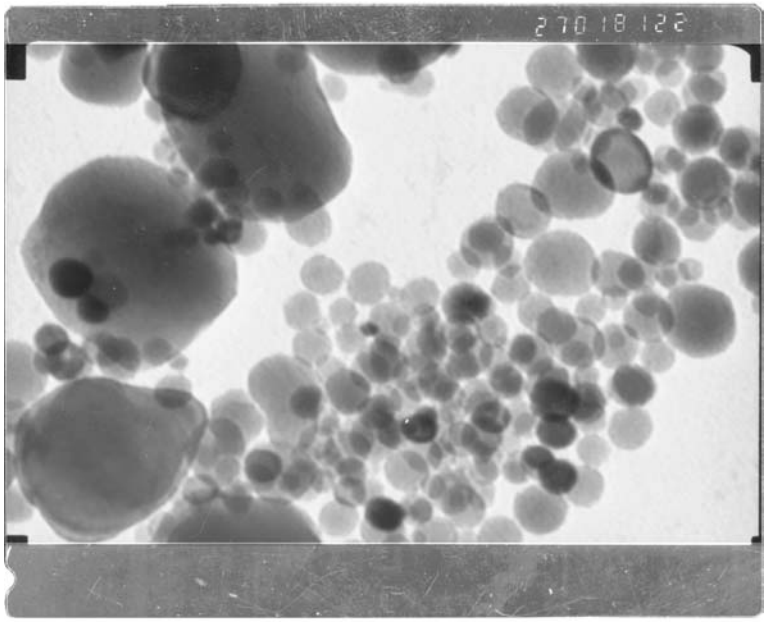

(b)

Figure 2 (a) Morphology of the secondary precipitates γ' (Magnification $\times$80,000). (b) Morphology of the tertiary precipitates γ' (Magnification $\times$270,000).

3.3. The effect of loading frequency

Presented in Fig. 4 are the crack growth rates obtained under triangular waveform at selected frequencies at 650°C as a function of ΔK. Mid-range crack growth has been achieved and the crack growth rate increases with decreasing frequency. The rate of the increment seems to be similar at both ΔK values, as indicated by the almost parallel lines across the two set of data points.

Crack growth rates at $\Delta K = 30$ and 40 MPa$\sqrt{\text{m}}$ were extrapolated at selected frequencies and a fracture mechanism map was constructed, as shown in Fig. 5. A slop of -0.25 was obtained from a best fit line through the data at $\Delta K = 30$ MPa$\sqrt{\text{m}}$ while -0.28 was obtained from the data at $\Delta K = 40$ MPa$\sqrt{\text{m}}$, indicating a mixed cycle/time dependent crack growth. Also included in the diagram are the crack growth rates at room temperature, representing the pure cycle-dependent crack growth. The transitional frequencies from mixed to cycle dependent crack growth may be estimated as 10 Hz at $\Delta K = 40$ MPa$\sqrt{\text{m}}$ and close to 200 Hz at $\Delta K = 30$ MPa$\sqrt{\text{m}}$. No region of time-dependent crack growth can be identified.

At 725°C, the crack growth rates extrapolated at $\Delta K = 30$ and 40 MPa$\sqrt{\text{m}}$ are presented in Fig. 6, to which the crack growth rates at room temperature are added also. An increased slop (-0.4) was observed, although the data can still be described by a single best fit line, indicating the dominance of a mixed cycle/time dependent crack growth mechanism. The differences between the crack growth rates obtained at $\Delta K = 30$ and 40 MPa$\sqrt{\text{m}}$ are smaller, indicating

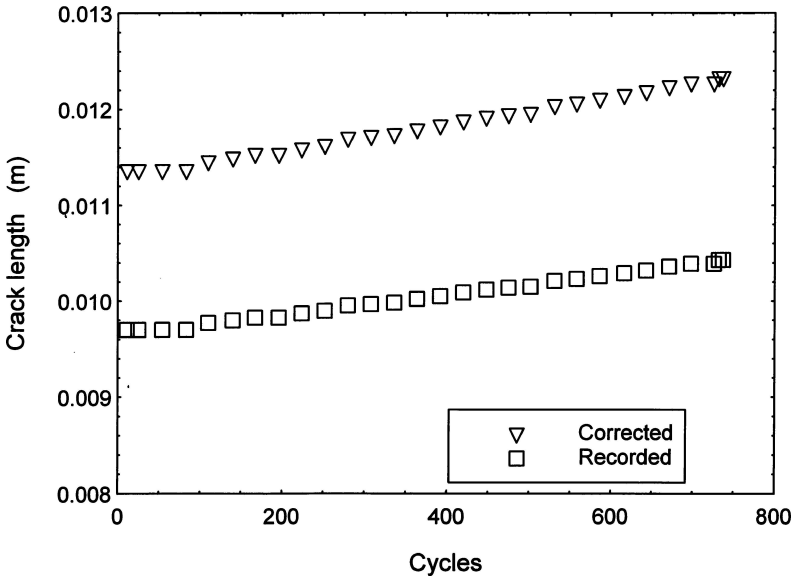

(a)

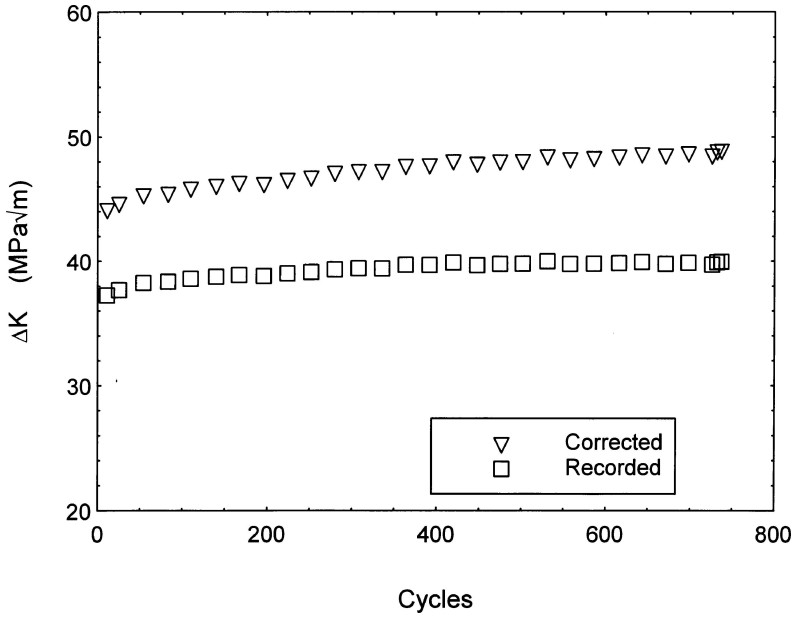

(b)

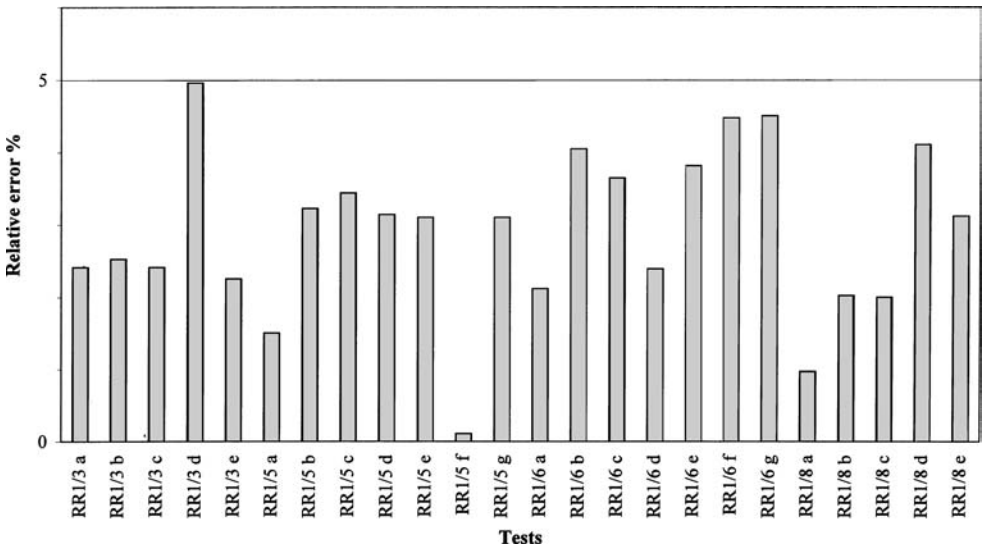

(c)

Figure 3 (a) Recorded and corrected crack length for a typical ΔK controlled test. (b) ΔK as a function of cycles, comparison of values obtained from recorded and corrected crack length. (c) Relative error of deviation of the corrected ΔK values from the desired value for a number of tests.

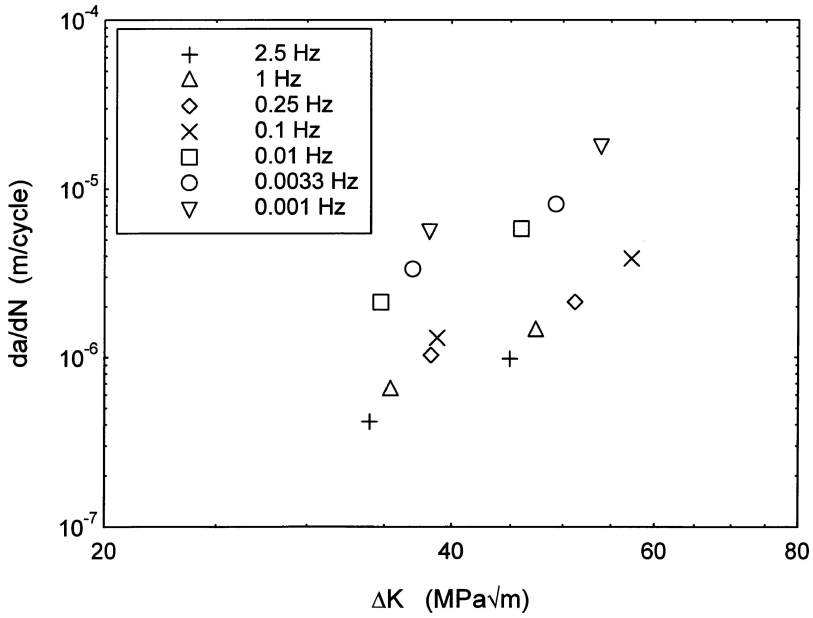

Figure 4 Fatigue crack growth rates as a function of ΔK for triangular waveform at 650°C.

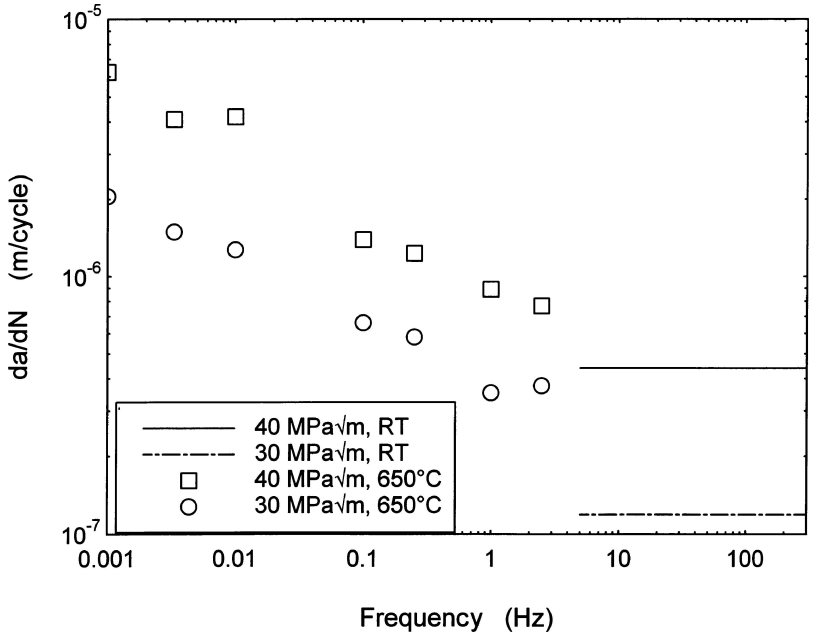

Figure 5 Fracture mechanism map for triangular waveform at 650°C (data obtained at 650°C except those at room temperature (RT)).

lower values of m in a Paris correlation, $\mathrm{d}a/\mathrm{d}N = C\Delta K^{\mathrm{m}}$. The transitional frequencies from mixed to cycle dependent crack growth are approximately 10 Hz at $\Delta K = 40$ MPa$\sqrt{\mathrm{m}}$ and 80 Hz at $\Delta K = 30$ MPa$\sqrt{\mathrm{m}}$, suggesting only a weak dependency of the temperature compared with the transitional frequencies at 650°C.

3.4. The effect of loading waveform

The crack growth was examined at 650 and 725°C under fast-slow, slow-fast and dwell waveforms. Fig. 7 shows the crack growth rates for all waveforms at $\Delta K = 40$ MPa$\sqrt{\mathrm{m}}$, including triangular, fast-slow, slow-fast and dwell at the maximum load at 650°C (a) and 725°C (b). A general trend appears to emerge: The crack growth rates under slow-fast waveform correlate well with those under triangular waveform for all the frequencies studied. While crack growth rates under dwell compare reasonably well with those under slow-fast and triangular waveforms up to ≈0.01 Hz, the increase in crack growth rates is evident for those with a hold period longer than 100 s. For fast-slow waveform, the crack growth rates seem to be almost constant, irrespective of the base loading frequency, particularly at 650°.

These results seem to suggest that for slow fast, triangular and dwell loading cases, the effect of waveform on crack growth rate is minimal for base frequencies $f \geq 0.01$ Hz. Dwell loading condition is the worst case for a hold period of longer than 100 s. The almost constant crack growth rate for fast-slow waveform seems to suggest that loading time may be critical in controlling the crack growth.

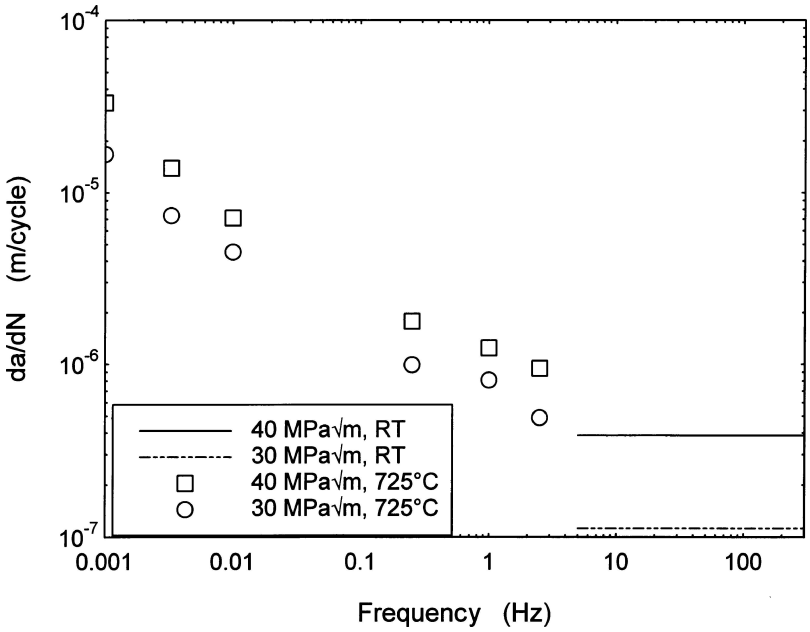

Figure 6 Fracture mechanism map for triangular waveform at 725°C (data obtained at 725°C except those at room temperature (RT)).

3.5. Time-dependent crack growth

Crack growth under sustained load was obtained at 650 and 725°C. Crack growth time rates for all waveforms are presented in Fig. 8, as a function of base frequency f. At $f < 0.01$ Hz, crack growth time rates under dwell loading are clearly higher than those under the other waveforms and comparable with those under sustained load [16].

Out-of-plane crack growth was observed under long dwell ($t_2 > 100s$) and sustained loading conditions, similar to that reported in U720Li alloy [17]. When the crack growth is of a mixture of tensile and shear modes, the crack growth rate data would be invalid according to ASTM E647-95a [14]. For comparison purposes, these data were also presented based on a finite element analysis [17]. The stress intensity factors K_{I} and K_{II} for a typical non-coplanar crack growth were calculated and the values of K_{I} were found to compare favourably with those of K_{I} for a projected crack on the plane of symmetry. The crack growth rates for out-of-plane crack growth were estimated in this manner [16] and included for comparison purposes.

4. Discussion

4.1. Metallurgical factors

Crack growth at elevated temperature is known to be strongly dependent on the chemical composition and microstructure of the material. Table II shows the comparison of the microstructural details for Alloy X, U720Li [18] and Waspaloy [19]. Whilst Alloy X and U720Li are both fine-grained PM alloys obtained by a similar solution and heat treatments, Waspaloy is a conventional course-grained alloy with low precipitates and almost no grain boundary carbines. Fig. 9 shows a comparison of crack growth rates in Alloy X, U720Li and Waspaloy for triangular (a) and dwell (b) waveform. Clearly, Alloy X exhibits the best crack growth resistance, closer to that of Waspaloy than that of U720Li. This is somewhat intriguing as U720Li is a fine-grained PM alloy with a similar chemical composition and heat treatment to that of Alloy X, while Waspaloy is a conventional cast-wrought alloy with much lower tensile strength and creep resistance (Table I). It seems that minor modifications in chemical composition and heat treatment may have been responsible for the improved crack growth resistance in Alloy X.

TABLE II Comparison of microstructural details of Waspaloy [19], U720Li [18] and Alloy X

Material	Grain size (μm)	Secondary γ' (nm)	Tertiary γ' (nm)
Waspaloy	100–200	50	30
U720Li	6	102	16
Alloy X	3.84	224	74

Although the exact mechanism of chemistry in improving crack resistance is not fully understood, the effects of some elements on crack growth have been noted for some time. For example, element Al and Ti were considered to be critical in the formation of the strengthening precipitates [1]. Cobalt and molybdenum were found to be beneficial and only minor addition of boron and zirconium can significantly improve the crack growth resistance [20]. Gayda *et al.* [21] studied the effects of boron and zirconium on crack growth in Waspaloy. They found that although the yield and ultimate tensile strength were unaffected by lowering B and Zr concentration, the fatigue crack growth rate increased three fold at $f = 0.33$ Hz and more than one order of magnitude at 120 s dwell in air. Compared with U720Li and Waspaloy, Alloy X contains a higher level of cobalt, molybdenum, titanium and zirconium, which may have contributed to the improved crack resistance at elevated temperature.

Complex heat treatments may be used to produce the optimal grain structure and the desired volume and size of the strengthening precipitates [20–22]. Grain size

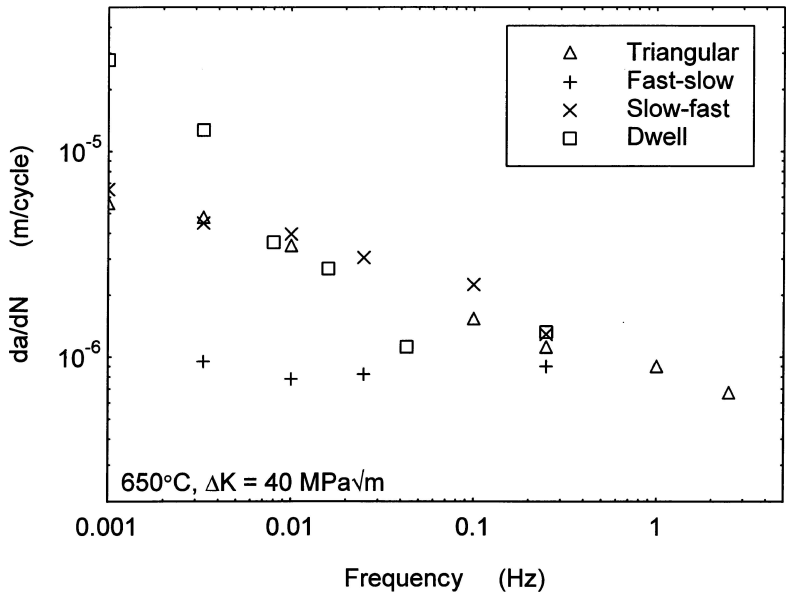

(a)

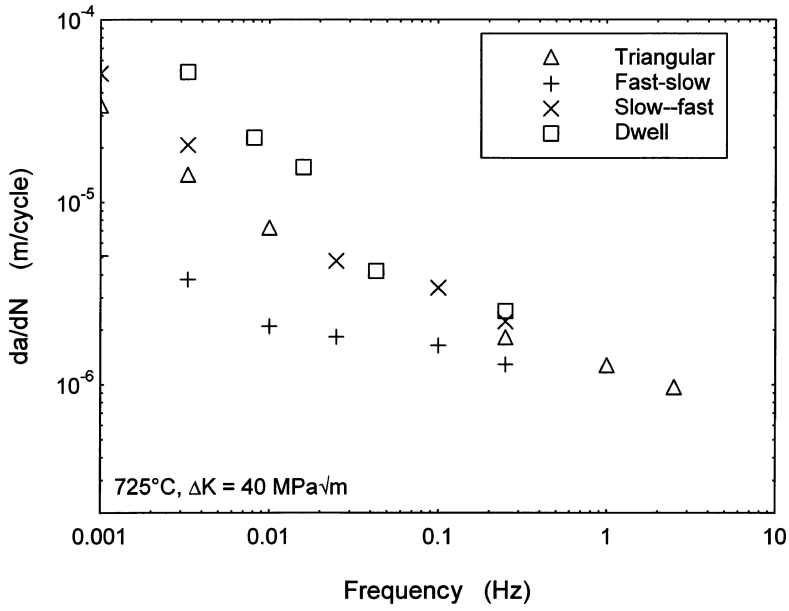

(b)

Figure 7 (a) Fracture mechanism map for all waveforms at 650°C, $\Delta K = 40$ MPa$\sqrt{}$m. (b) Fracture mechanism map for all waveforms at 725°C, $\Delta K = 40$ MPa$\sqrt{}$m.

may affect the extent of grain boundary crack growth by preferential grain boundary oxidation. Gayda and Miner [21] studied a PM nickel-based superalloy, Astroloy, at 650°C by varying the grain size and the size and distribution of the strengthening γ' phase. They found that a fine grain size promoted rapid intergranular crack growth while a coarse grain promoted slower, trans-granular crack growth. On the other hand, the size and distribution of precipitates influence the slip character hence must be considered also. The presence of small, coherent particles are easily shearable hence in favour of planar slip deformation. In contrast, large, nonshearable precipitates promote wavy slip corresponding to more uniformly distributed dislocation arrangements, favoured by low frequency and low strain rates [20]. Jackson and Reed [22] show that optimum properties may be obtained when the precipitates are of a size which maximises the resistance to cutting by weakly coupled dislocation pairs based on theories of precipitation hardening. The average grain size of Waspaloy is about 100 μm with a low volume of coherent small γ' precipitates that are mostly shearable. In Alloy X, although the average grain size is much smaller, the distribution and the size of the precipitates are optimised so that both the grain boundaries and the matrix become stronger at elevated temperature. This may be the prime reason why a predominant mixed trans and inter-granular crack growth is observed in Alloy X and largely intergranular crack growth in Waspaloy for a given frequency or waveform. Since U720Li alloy was strengthened in a similar manner, a similar mixed behaviour was observed [5] for the same frequency range, although the sizes of the secondary and tertiary γ' in U720Li alloy are smaller

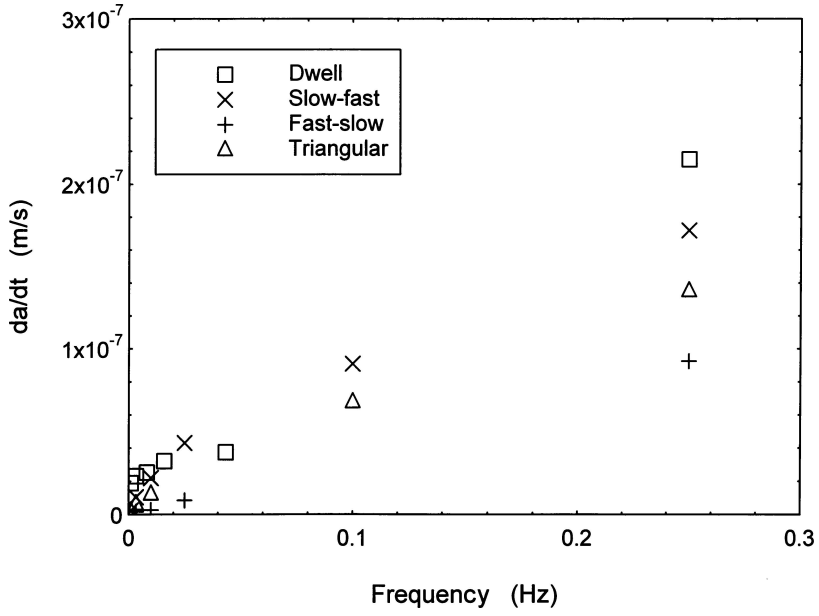

(a)

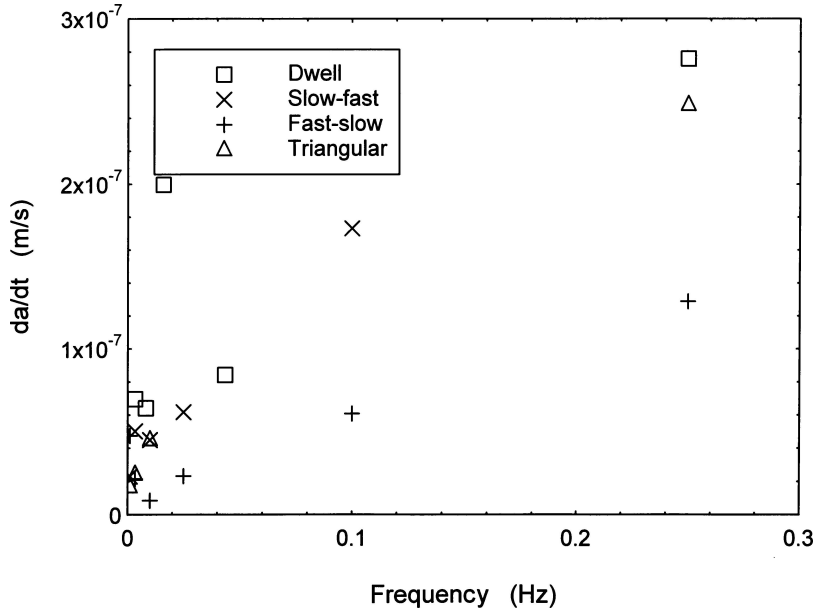

(b)

Figure 8 (a) Crack growth time rates as a function of frequency at 650°C, $\Delta K = 30$ MPa$\sqrt{}$m. (b) Crack growth time rates as a function of frequency at 725°C, $\Delta K = 30$ MPa$\sqrt{}$m.

compared with those of Alloy X, a fact that may have contributed to the difference in the fatigue crack growth resistance of the two alloys, in addition to the variation in composition.

The predominant mixed time/cycle dependent crack growth is clearly due to the effective grain boundary strengthening. Interestingly, however, a slope of –0.3 to –0.4 seems to be common to a range of nickel-based alloys in a log-log crack growth rate versus frequency plot [5].

4.2. The influence of creep deformation

For dwell waveform, the crack growth rate increases significantly when $t_2 > 100s$ and the crack growth time rates become comparable to those under sustained load. This time dependency of crack growth may be due to creep and/or oxidation. The contribution of creep deformation was evaluated by monitoring the load-line displacement during tests under sustained loading, representing the limiting condition of long dwell tests. Fig. 10 show the components of load-line displacement (a) and displacement rates (b) at 650°C. The total displacement was obtained from the extensometer readings while the elastic component was obtained from an elastic analysis [23]. The displacement due to creep was then estimated by removing the elastic portion from the total deflection. It seems immediately clear that the creep deformation during the crack growth is extremely limited. This is further supported by the lack of any physical evidence of creep damage during post-test examination of the fracture surfaces. This feature will be further explored in Part II and Part III of this paper.

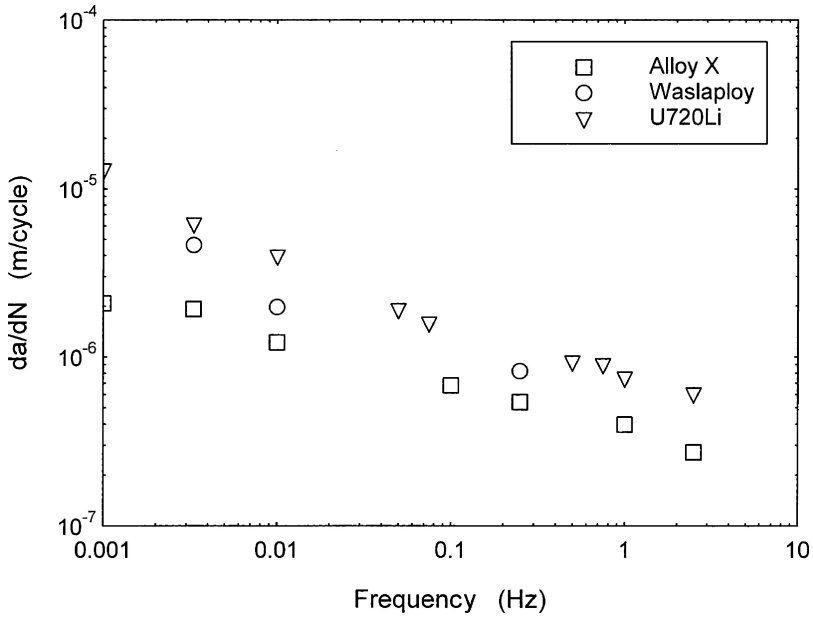

(a)

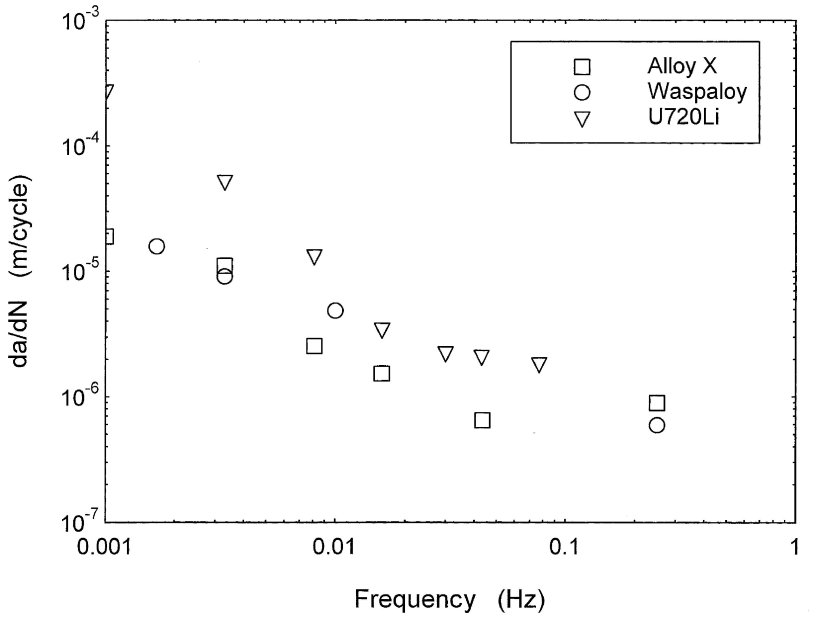

(b)

Figure 9 (a) Comparison of crack growth rates of Alloy X, U720Li and Waspaloy under triangular waveform at 650°C, $\Delta K = 30$ MPa$\sqrt{}$m. (b) Comparison of crack growth rates of Alloy X, U720Li and Waspaloy under dwell waveform at 650°C, $\Delta K = 30$ MPa$\sqrt{}$m.

4.3. The role of crack tip constraint

At elevated temperature, the crack growth patterns may differ significantly from those at room temperature, particularly for predominantly time-dependent crack growth. The out-of-plane crack growth observed in Alloy X and U720Li [17] is one of them. A plausible reason may be the directional stability argument offered by Cotterell [24]. The directional stability relies on the stress state, or the constraint, near the crack tip. The crack tip constraint is usually represented by the elastic T-stress. With a high positive T-stress in CT specimens, the crack path is inherently unstable if a small excursion becomes available [17]. Such excursions may be readily available for predominantly intergranular crack growth at elevated temperature. If the actual excursion from the ideal path may be assumed as in the same order as the plastic zone size, then the excursion may be in the range of 40 μm (at $\Delta K = 30$ MPa$\sqrt{}$m) and 150 μm (at $\Delta K = 40$ MPa$\sqrt{}$m) for Alloy X. This means that the plane strain plastic zone would encompass between 6 to 21 grains, sufficient to weaken the grain boundaries near the crack tip. The initial excursion may be regulated by the orientation and size of the grains with respect to the crack tip and subsequent crack growth will be influenced by the combined effect of plasticity and oxidation. Oxygen may gain easy access into the selected grain boundaries along the plastically deformed area hence facilitate the unstable crack growth. Such out-of-plane crack growth has not been reported in conventional alloys such as Waspaloy. The average grain size in conventional alloys will be in the same order as that of the plastic zone size, consequently the

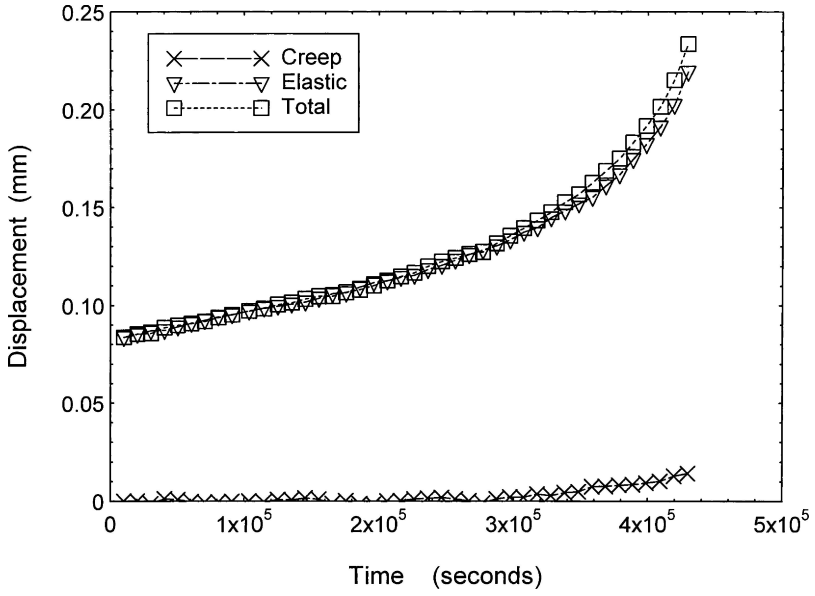

(a)

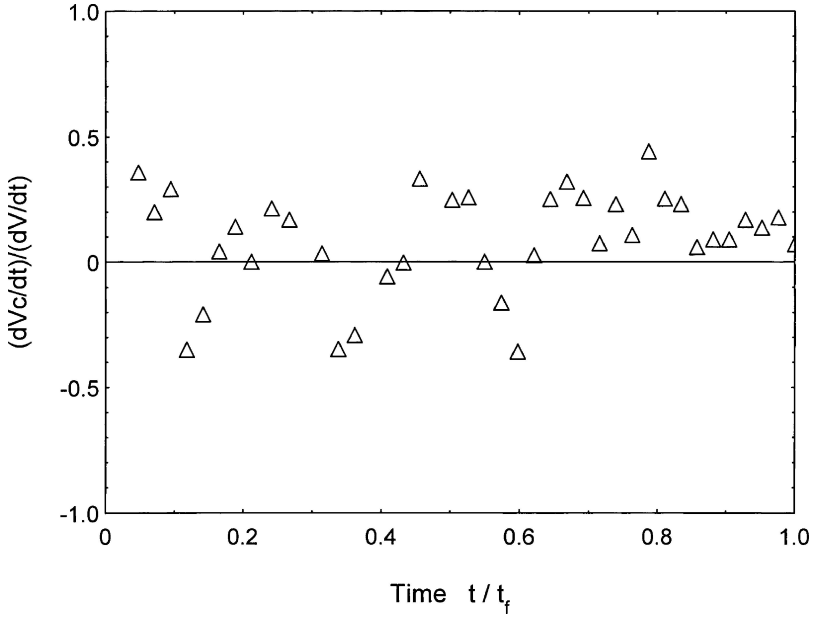

(b)

Figure 10 (a) Components of load-line displacement and (b) load-line displacement rates as a function of time at 650°C.

role of plasticity would be far less significant in controlling the grain boundaries hence the direction of the crack growth.

5. Conclusions

The following conclusions may be drawn from this work:

1. The effect of loading waveform seems to be minimal for base frequency $f > 0.01$ Hz. A mixture of time and cycle dependent crack growth was observed for all waveforms except the fast-slow waveform, where the crack growth remained cycle dependent and the crack growth rate mostly constant.

2. For base frequency $f \leq 0.01$ Hz, crack growth rates under dwell waveform increased significantly and became comparable to those under sustained load.

3. Creep deformation was found to be limited for the sustained loading cases at 650 and 725°C in this alloy. It seems reasonable to assume that the role of creep in crack growth is insignificant for this alloy under the test conditions examined.

4. Crack tip constraint may be responsible for the out-of-plane crack growth observed under predominant sustained loads.

Acknowledgements

This work was supported by the Engineering and Physical Science Research Council (EPSRC) of UK (GR/M44811). SD was partially sponsored by DERA (now QinetiQ). Specimens were provided by Rolls-Royce plc. The authors are grateful for the technical support from Prof. G Harrison and Dr. M. Henderson (QinetiQ) and Dr. M. C. Hardy and Dr. I Hussey

(Rolls-Royce plc.); for the assistance of Mr. C. Lupton in the experimental work.

References

1. J. E. KING, *Mater. Sci. Tech.* **3** (1987) 750.
2. S. FLOREEN and R. H. KANE, *Fatigue Eng. Mater. Struct.* **2** (1980) 401.
3. M. R. WINSTON, K. M. NIKBIN and G. A. WEBSTER, *J. Mater. Sci.* **20** (1985) 2471.
4. T. WEERASOORIYA, in "Fracture Mechanics: Nineteenth Symposium," edited by T. A. Cruse (ASTM STP 969, 1988) p. 907.
5. J. TONG and J. BYRNE, *Fatigue Fract. Eng. Mater. Struct.* **22** (1999) 185.
6. F. V. ANTUNES, J. M. FERREIVA, C. M. BRANCO and J. BYRNE, *Mater. High Temp.* **17** (2000) 439.
7. J. GAYDA, T. P. GABB and R. V. MINER, in "Low Cycle Fatigue," ASTM STM **942** (1988) 293.
8. J. BYRNE, R. HALL and L. GRABOWSKY, in "Behaviour of Defects at High Temperature," (ESIS15, 1993) p. 367.
9. S. P. LYNCH, T. C. RADKE, B. J. WICKS and R. T. BYRNES, *Fatigue Fract. Engng. Mater. Struct.* **17** (1994) 97.
10. N. E. ASHBAUGH, in 15th National Symposium on Fracture Mechanics, University of Maryland (1982).
11. A. PLUMTREE and S. SCHAFER, *Adv. Fract. Res.* **3** (1984) 2249.
12. H. GHONEM and D. ZHENG, *Mater. Sci. Engng*. A **150** (1992) 151.
13. V. HODKINSON, PhD thesis, University of Portsmouth, 1997.
14. ASTM E647-95, 1995.
15. ASTM E112-88, 1988.
16. S. DALBY, PhD thesis, University of Portsmouth, 2001.
17. J. TONG, *Fatigue Fract. Engng. Mater. Struct.* **24** (2001) 771.
18. N. J. HIDE, M. B. HENDERSON, A. TUCKER and P. A. S. REED, *ICM8* (1999) 429.
19. M. CLAVEL, C. LEVAILLANT and A. PINEAU, in "Creep-Fatigue-Environment Interactions" (Warrendale, PA, Metallurgical Society of AIME).
20. A. PINEAU, in "Flow and Fracture at Elevated Temperatures," edited by R. Raj (American Society for Metals), p. 317.
21. J. GAYDA and R. V. MINER, *Int. J. Fatigue* **5** (1983) 135.
22. M. P. JACKSON and R. C. REED, *Mater. Sci. & Engng.* A **259** (1999) 85.
23. T. L. ANDERSON, "Fracture Mechanics: Fundamentals and Applications" (CRC Press, 1995).
24. B. COTTERELL, *Int. J. Fract. Mech.* (1966) 526.

Received 8 October 2003
and accepted 24 September 2004